Journal of The Electrochemical Society, **155** (2) A181-A188 (2008)
0013-4651/2007/155(2)/A181/8/$23.00 © The Electrochemical Society

Study of Germanium as Electrode in Thin-Film Battery

B. Laforge,[a] L. Levan-Jodin,[a,z] R. Salot,[a] and A. Billard[b]

[a]*CEA, F–38054 Grenoble Cedex, France*
[b]*LERMPS-UTBM, F–90010 Belfort Cedex, France*

Sputter-deposited gemanium thin films were investigated as negative electrode material for lithium-ion batteries. X-ray diffraction, scanning electron microscopy, and secondary-ion mass spectroscopy have been carried out. Doped and nondoped films were cycled vs lithium electrode. Diffusion coefficients, reaction potential, and cycling life were measured. The effect of doping and electrode thickness was also studied. The stable capacity is ~1460 mAh g^{-1}, with an increase over the 180 first cycles for n-doped germanium coatings.
 [DOI: 10.1149/1.2820666]

Manuscript submitted August 30, 2007; revised manuscript received October 30, 2007.
Available electronically December 19, 2007.

For the miniaturization of Li batteries, a number of studies have been carried out on electrode and electrolyte thin films. For anodic electrodes, the elements of group IV (Si, Ge, Sn, Pb) arouse interest due to their large theoretical capacity.[1-4] Most of the commercial rechargeable Li ion batteries are based on graphite, and the complete lithiation of graphite in LiC_6 results in a theoretical capacity of 372 mAh g^{-1} while the theoretical capacity of silicon is 4200 mAh g^{-1}. However, the elements of group IV have a major drawback as anode materials; they constantly undergo substantial expansion/contraction during the charging/discharging processes. The resulting stress tends to depreciate the host after a few cycles. However, in thin-film batteries, the effect of volume change is expected to be less.

Silicon arouses interest because of its very high theoretical capacity, but an analogous system, Li–Ge, has been poorly studied.[5] The theoretical capacity of this system is ~40% that of Li–Si (1600 mAh g^{-1}), and its cost is higher, but the main interest of germanium comes from its diffusion coefficient and its good cycling life.[6,7] According to Fuller and Severiens,[8] the diffusion coefficient of lithium in germanium is about two orders of magnitude higher than in silicon. This work will focus on the electrochemical characterization of germanium thin layers, which could be a promising negative electrode material in thin-film batteries.

Experimental

Germanium thin films were prepared by radio-frequency (rf) magnetron sputtering on Cu substrates. The experimental device was an Alcatel SCM 640 sputtering chamber pumped down via a turbomolecular pump, allowing a base vacuum of ~10^{-4} Pa. The 150 mm diam target was powered by a 200 W rf supply. The flow rates of argon and oxygen were controlled with MKS flowmeters and the total pressure was measured using an MKS Baratron gauge. The Cu foil substrates were disposed next to the target at a distance of 95 mm. The argon pressure was maintained at 0.1 or 2 Pa. The deposition rate was ~30 nm min^{-1}, whatever the pressure. Doped and nondoped germanium targets were used. The nondoped germanium target came from a germanium single crystal. The doped targets were boron doped for the p-type and phosphorus doped for the n-type. Boron and phosphorus concentrations were 10^{20} atom cm^{-3}. The targets were prepared by hot pressing of doped powders; 99.99 and 99.999% pure powders were used for the p-doped and n-doped targets, respectively.

Scanning electron microscopy (SEM) was performed using a FEG LEO 1530 operating at 5 kV. Brittle-fracture cross sections were also performed on 1 μm thick germanium coatings deposited on silicon wafers to investigate their morphology. Low angle X-ray diffraction (XRD) analyses were done with a Siemens D5000 diffractometer using the Cu Kα radiation (λ = 0.15406 nm). The corresponding samples were deposited on glass substrates, and the diffraction spectra were acquired in air. The chemical compositions were determined from 200 nm thick (p-doped) and 450 nm thick (n-doped) germanium coatings deposited on silicon wafers by secondary-ion mass spectroscopy (SIMS) analysis. Cs^+ ions (15 keV) and O_2^+ ions (5 keV) have been used for the p-doped and n-doped germanium coatings, respectively. The accuracy of these SIMS measurements was estimated at ~10%, depending on impurities combination into the matrix.

The coatings were packaged in button or Swagelock cells without air contact and assembled in an Ar-filled glove box. The cells were composed of a metallic lithium foil, a porous polypropylene separator (celgard 2400), and the copper foil coated with germanium as the working electrode. Germanium electrodes were stored in a glove box. The electrolyte was $LiPF_6$ in a 1:1 mixture of ethylene carbonate (EC) and diethylene carbonate (DEC).

The galvanostatic intermittent titration technique (GITT) has been used to perform diffusion coefficient measurements. Current jumps are 10 μA for 30 min with a time relaxation of 2 h. The samples were button cells with a 200 nm thick germanium film and lithium metal as counter electrode.

Voltage profiles have been measured between 0.05 and 1.5 V vs Li/Li^+. (All voltages in the paper refer to the Li/Li^+ reference electrode). Cyclic voltammograms from 1.5 to 0.05 V with a scan rate of 20 μV s^{-1} were done. Charge/discharge capacity tests were performed at several current densities. Cycling life has been measured with a constant current of 100 mA cm^{-1}. An Arbin Instruments BT 20001 battery cycler was used for the charge/discharge capacity and galvanostatic measurements. The GITT experiments and cyclic voltammetry were performed with a Biologic VMP 2.

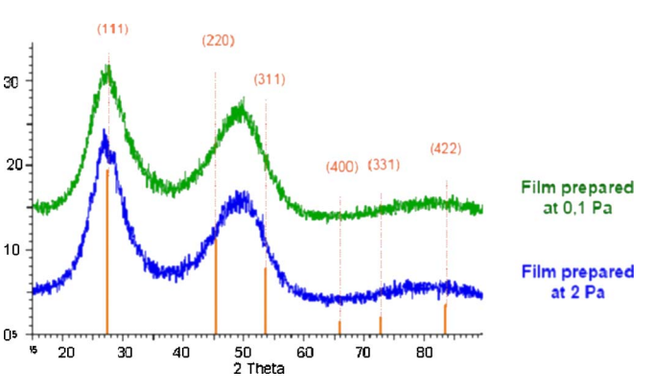

Figure 1. (Color online) XRD patterns of p-doped germanium coatings deposited at low (0.1 Pa) and high (2 Pa) argon pressures.

[z] E-mail: lucie.levan-jodin@cea.fr

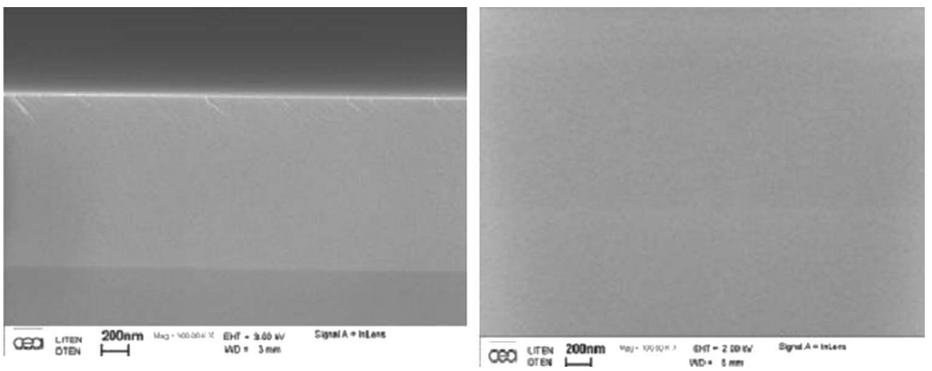

Figure 2. Brittle fracture cross section (left) and top surface (right) SEM micrographs of a 1 μm thick p-doped germanium film deposited at 0.1 Pa Ar.

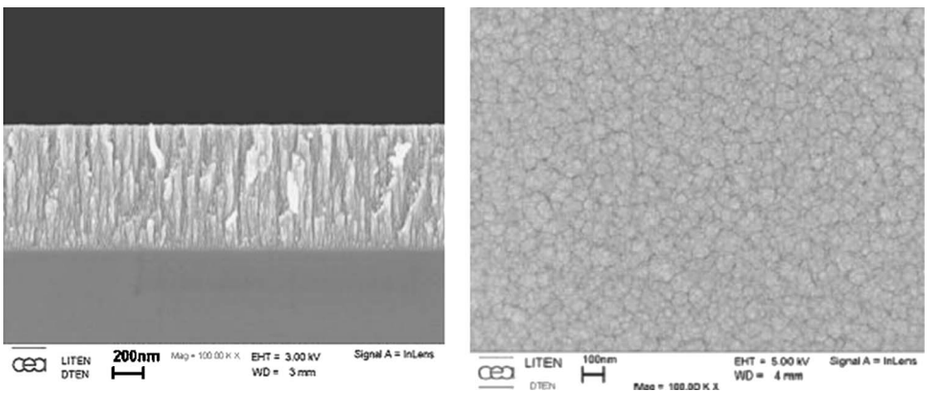

Figure 3. Brittle fracture cross section (left) and top surface (right) SEM micrographs of a 1 μm thick p-doped germanium film deposited at 2 Pa Ar.

Results

Structural, chemical, and morphological characterizations.— XRD patterns of p-doped germanium deposited at 0.1 and 2 Pa of Ar are presented in Fig. 1. The two patterns are similar and typical of amorphous (or very badly crystallized) materials. Then, the pressure does not have any influence on the crystallinity of sputter-deposited germanium.

SEM has been used to observe the influence of the working pressure on the density of ~1 μm thick germanium films. The coating deposited at low pressure (0.1 Pa) exhibits a glassy aspect brittle fracture cross section characteristic of dense and amorphous films (Fig. 2). Its top surface observation shows a very smooth surface without visible growth defect. The films elaborated at 2 Pa displays a columnar morphology and a rough surface (Fig. 3). The column's diameter is about 10–200 nm.

Because germanium films have been studied to be integrated into a thin-film solid-state battery, we will focus only on the coatings deposited at 0.1 Pa films because their denser and smoother aspect is expected to be better for integration. Indeed, a solid electrolyte will be deposited on germanium, and it will be easier on a smooth surface than on a rough surface.

SIMS concentration profiles performed on boron and phosphorus through the whole thickness of the n- and p-doped films (Fig. 4) indicate that the doping element concentration is constant. The peak at the germanium/silicon interface is a measurement artifact that might come from the presence of a little amount of oxygen due to the absence of surface ion cleaning prior to the deposition stage.

Concentrations of doping elements measured by SIMS are presented in Table I. The concentration of the targets given by the manufacturer without an analysis certificate was $\sim 10^{20}$ atom cm^{-3}, but the doping rates of deposited films are about 6.7×10^{18} atom cm^{-3} for the n-doped and 5.5×10^{19} atom cm^{-3} for the p-doped. The spatial distribution of sputtered metal atoms, mainly a function of the impinging argon ions energy and of the atomic number of the target elements, cannot be involved to explain such differences between the composition of the target and that of the coating. Indeed, this phenomenon often yields composition discrepancies of some tens of percents.[9-11] It can thus be concluded that the target's doping rates of $\sim 10^{20}$ atom cm^{-3} given by the manufacturer are not available.

Electrochemical measurements.— GITT measurements.— The diffusion coefficients of Li in Ge by GITT measurements are reported in Fig. 5 vs Li rate into Li_xGe coatings. It is necessary to be careful with GITT results because the error factor can be relatively high, especially at low Li content. The diffusion coefficients of doped or nondoped germanium are very similar. At low Li concentrations, the diffusion coefficient is around 1.5×10^{-10} cm^2 s^{-1} but the more germanium is lithiated, the lower the diffusion coefficient. For highly lithiated compounds, the diffusion coefficient is about

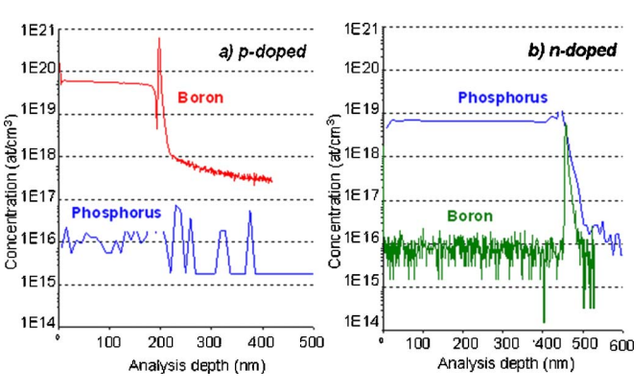

Figure 4. (Color online) SIMS concentration profiles of p-doped (a) and for n-doped (b) germanium coatings.

Table I. Concentrations of doping elements in doped germanium films.

	Phosphorus concentration (atom cm^{-3})	Boron concentration (atom cm^{-3})
p-doped film	1.3×10^{16}	5.5×10^{19}
n-doped film	6.7×10^{18}	8.4×10^{15}

5×10^{-12} cm^2 s^{-1}. It is interesting to note that differences between diffusion coefficients of Li^+ in doped and nondoped germanium are observed only at low lithium rates (1.41×10^{-10} cm^2 s^{-1} for nondoped Ge and 1.75×10^{-10} cm^2 s^{-1} for n-doped Ge at $x = 0.3$).

Voltage profile.— The voltage profile (Fig. 6) and differential capacity (Fig. 7) have been done on a 200 nm thick p-doped germanium film prepared at 0.1 Pa. The imposed current density is 10 μA cm^{-2}, which corresponds to a cycling rate of C/15. The evaluation of the germanium mass has been calculated from the thickness of the film, the surface of the electrode, and the theoretical germanium density ($d_{Ge} = 5.323$ g cm^{-3}). This evaluation is probably very close to the real value because the germanium film appears dense on SEM images (see Fig. 2). The voltage profiles of doped or nondoped germanium are similar; that is why most of results will be given only for p-doped films. The first, second, and tenth cycles are used to determine the approximate potentials where different reactions, i.e., solid electrolyte interface (SEI) formation and lithium intercalation, occur.

The initial lithiation of germanium begins by a voltage plateau at 0.6 V (I in Fig. 6 and 7). As this plateau exists only during the first discharge, it is probably due to the formation of a SEI. As $LiPF_6$, EC, and DEC are contained in the electrolyte, SEI will be mainly formed by Li_2CO_3, C_2H_5COOLi, and LiF. This hypothesis is confirmed by the irreversible lithiation during the first cycle where 0.5 atom Li/atom. Ge is trapped into the electrode. The plateau is followed by two pseudoplateaus (II in Fig. 6) corresponding to two large peaks, around 0.35 and 0.18 V (Fig. 7). They could display single-phase regions where amorphous germanium is lithiated or may come from a heterogeneous material with a succession of Li–Ge amorphous or crystalline phases. Below 0.1 V, the voltage decreases more quickly. The end of the first discharge corresponds to a compound with ~4.5 atom Li/atom Ge.

The delithiation results in two pseudoplateaus (III and IV), which are characterized by two very large modulations visible in Fig. 7, around 0.4 and 0.7 V, corresponding to single-phase regions or heterogeneous materials, as involved in the discharge behavior description. During the second discharge, a pseudoplateau (IV) appears as in the first discharge. The number of lithium atoms involved in the reversible germanium lithiation and delithiation is only ~3.9 atom Li/atom Ge. That is equivalent to a reversible capacity of 1470 mAh g^{-1}. Among the phases of the Li–Ge system, the stoichiometries that should correspond are $Li_{15}Ge_4$ or Li_7Ge_2.[12-15] However, there is no plateau during the discharge, which could be the consequence of the delithiation of a crystallized single phase. These results are in agreement with those of Graetz et al.[6] who observed the presence of amorphous and crystallized phases on delithiated germanium by XRD.

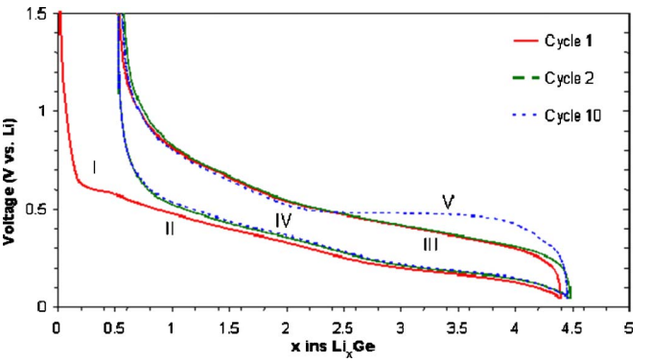

Figure 6. (Color online) Voltage profiles vs x (x = Li rate in Li_xGe phases) for different cycle numbers of a 200 nm thick p-doped germanium film.

During the tenth cycle, the discharge curve overlays the previous ones, but the charge behavior evolves. Figure 6 exhibits a plateau at ~0.5 V (V), probably due to a two-phase region and/or the formation of crystalline phases, followed by a pseudoplateau identical to that of the other cycles.

Cyclic voltammetry.— Cyclic voltammetry measurements have been performed for 10 cycles to study the influence of the cycle number and of the thickness of Ge films on their performances. In Fig. 8, the behaviour of a 400 nm thick film is reported. During the first discharge, besides the SEI peak at 0.6 V, two little peaks are present at about 0.3 and 0.1 V, but they tend to disappear during further cycles while new well-defined peaks appear. At the end of the tenth cycle, voltammograms are stable and present three peaks at 0.5, 0.35, and 0.18 V. Two very large peaks are detectable during the first and second charges at 0.4 and 0.7 V. After the fifth dis-

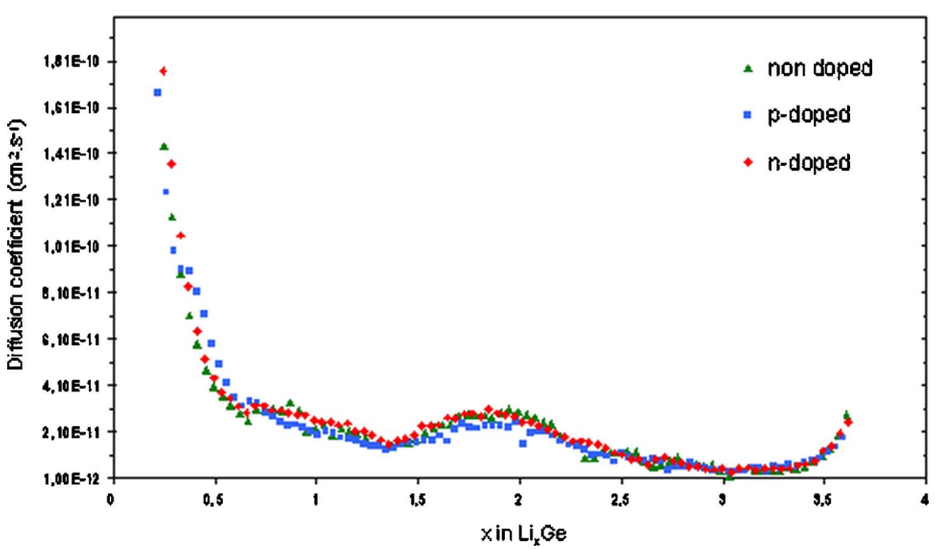

Figure 5. (Color online) Diffusion coefficient of Li vs x in Li_xGe for nondoped, p-doped, and n-doped germanium coatings.

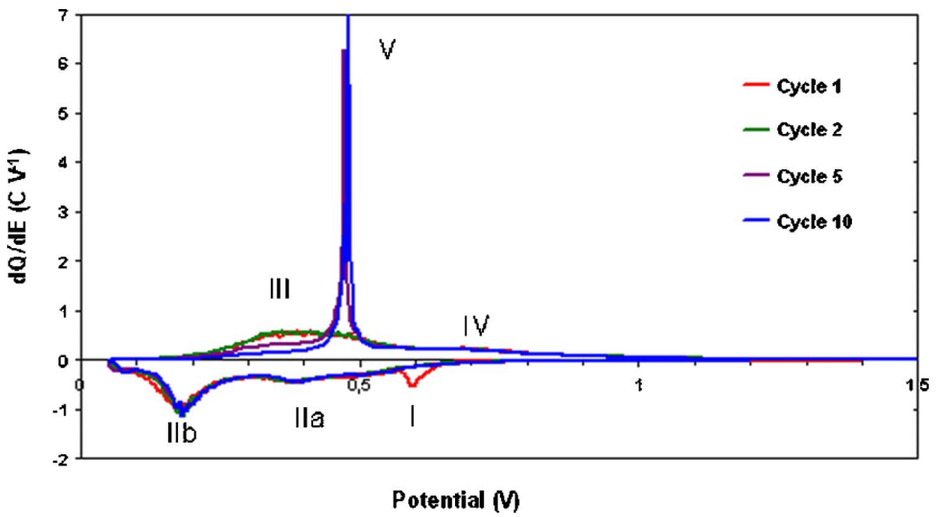

Figure 7. (Color online) Differential capacity vs voltage for a 200 nm thick p-doped germanium film.

charge, the 0.4 V peak intensity decreases but a new fine peak appears at about 0.5–0.6 V. At the tenth cycle, the 0.4 V peak completely disappeared but there is still a very fine well-defined peak at 0.6 V.

This experiment has been repeated in the same conditions for germanium electrode coatings of various thicknesses: 50, 100, 200, and 400 nm. The behavior of the 200 nm thick film is similar to that of the 400 nm thick described above.

Results obtained on the 50 nm thick film are plotted in Fig. 9. All the curves are perfectly superimposed, except for the first discharge where a small peak at 0.6 V is visible and disappears at the second discharge. This peak is attributed to the SEI formation. The electrochemical voltages relative to the peaks of the 50 nm thick Ge coating are similar to those observed for the tenth cycle of the 400 nm thick electrode (i.e., 0.5, 0.35, and 0.18 V during the discharge and 0.55 and 0.7 V during the charge).

The voltammograms of coatings with four thicknesses are reported in Fig. 10 for the third cycle. It exhibits the influence of the thickness in germanium electrodes cycling. The thinner the film is, the earlier the 0.5 V peak during the charge appears. While increasing the Ge film thickness, the most important peak during the discharge increases from ~0.18 V to ~0.1 V. This phenomenon is attributed to the compressive stress level into the films, which increases with the coating thickness.[16] During the cycling, the germanium structure is modified.

Cycling life: p-doped.— In Fig. 11, the discharge capacity per volume unit vs the cycle number has been reported for three different thicknesses of p-doped germanium coatings and for several currents. At low current, the discharge capacity of the three films is almost the same: 800 μAh cm^{-2} μm^{-1} (~1500 mAh g^{-1}). This value is close

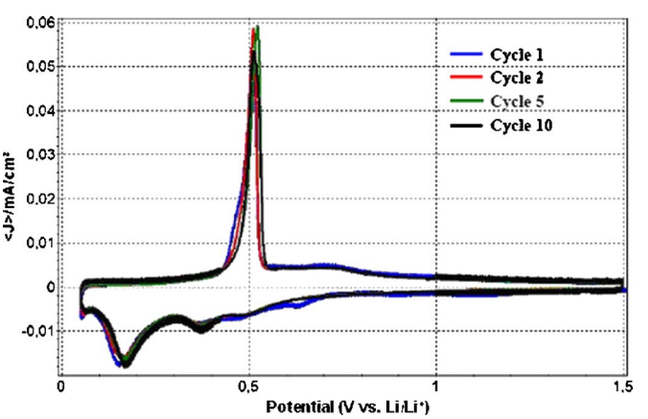

Figure 9. (Color online) Voltammograms of a p-doped germanium film (thickness: 50 nm) during the cycles 1, 2, 5, and 10.

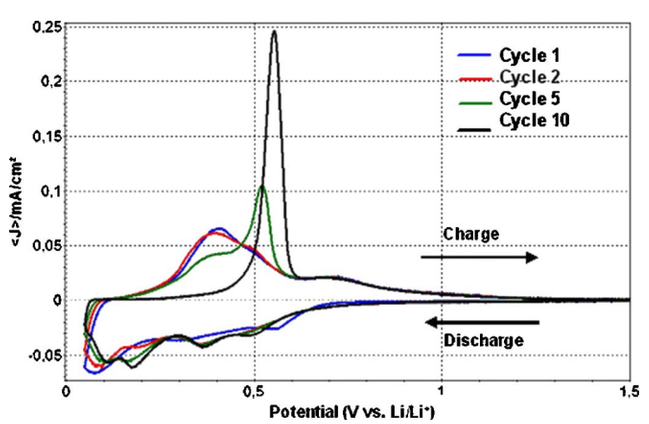

Figure 8. (Color online) Voltammograms of a p-doped germanium film (thickness: 400 nm) during the cycles 1, 2, 5, and 10.

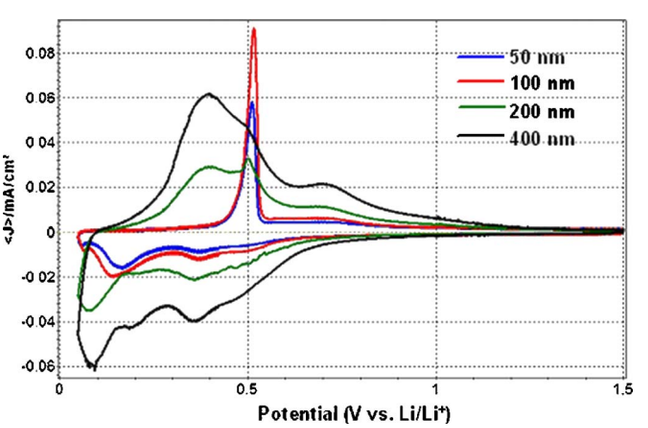

Figure 10. (Color online) Voltammograms achieved from the third cycle on p-doped germanium for several thicknesses (50, 100, 200, and 400 nm).

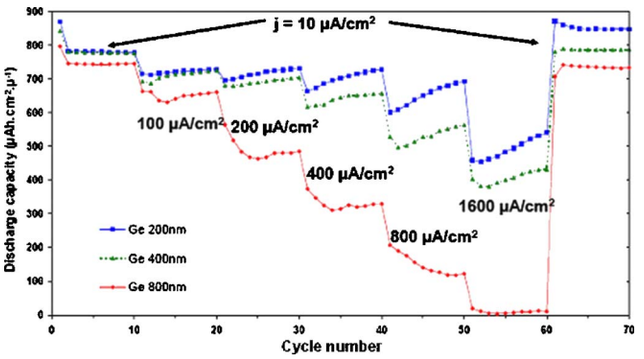

Figure 11. (Color online) Discharge capacities per volume unit for several thicknesses of p-doped germanium films vs cycle number and for several current densities.

to the theoretical one (1600 mAh g^{-1}). When the current increases, the capacity of the 800 nm thick Ge electrode dramatically decreases. For a current of 1600 µA cm^{-2}, its capacity is near zero while that of the 200 and 400 nm thick films is ~500 and ~400 µAh cm^{-2} $µm^{-1}$, respectively.

At the end of each set of experiments, the current was decreased to its initial value (i.e., 10 µA cm^{-2}). The capacity then also dropped to its initial value, ~800 µAh cm^{-2} $µm^{-1}$, even for the thicker coating. This means that the low capacity of the 800 nm thick electrode under high current densities is not due to its spoiling but to the cycling rate: when the cycling rate is too high, the thick germanium electrode is no more able to quickly insert lithium, which should be linked to the diffusion mechanisms of lithium in p-doped germanium.

Figure 12 exhibits the discharge capacity vs the cycle number for four germanium electrodes with a thickness ranging from 200 nm to 2 µm and with a current density of 100 µA cm^{-2}. The irreversible capacity of the first cycle, due to the SEI, is very low, <10% of the reversible capacity. The thinner the film is, the better the cycling behavior. For the 200 and 400 nm thick electrodes, the capacity even increases until ~100 cycles before it decreases. This enhancement should be explained by volume modifications during the lithiation/delithiation: cracks and porosity appear, inducing an increase of the active surface. Indeed, with such a rather high current density as 100 µA cm^{-2}, the effect of the diffusion cannot be neglected. The surface increase due to crack formation shortens the diffusion path, and lithiation is not more limited by the cycling rate. But on very thin films, the effects of the volume expansion are less important than on thick films.

The SEM images presented in Fig. 13 for a 200 nm thick coating confirm the assumption. After the first cycle, some cracks appear (Fig. 13a). A strong array of cracks develop over the whole surface of the coating after 10 cycles (Fig. 13b). Further cycles lead to an electrochemical grinding of the coating. After ~100 cycles, it defines islands of some micrometers in diameter (Fig. 13c), which strongly improves the active surface of the coating. The capacity decline observed in Fig. 12 after the 100th cycle could be explained by a degradation of the electrodes due to the cracks propagation, which leads to the shedding of the coating after 300 cycles (Fig. 13a).

Cycling life: n-doped.— The same study has been done on n-doped germanium electrodes with thickness in the range of 50–400 nm. The discharge capacity per volume unit vs the cycle number for several current densities is reported in Fig. 14. It shows that there is almost no difference of behavior, whatever the thickness of the film; although a significant difference was observed between 200 and 400 nm thick coatings synthesized with p-doped germanium. This phenomenon could be explained by a lower rate of lithium diffusion into p-doped germanium than into n-doped. For cycles 60–70, the capacities remain almost the same as for the first 10 cycles performed with the same discharge current of 10 µA cm^{-2}. This probably indicates that there is no deterioration of the electrodes during cycling at higher current densities.

The capacity under 100 µA cm^{-2} of n-doped films as a function of the cycle number is plotted in Fig. 15. The capacity remains stable up to ~180 cycles except for the thickest film, which is stable only up to ~100 cycles. Beyond 180 cycles, the capacity decreases.

Doping influence.— In order to understand the role of the doping, capacities and cycling lives of 400 nm thick p-doped, n-doped, and nondoped germanium coatings are compared (see Fig. 16 and 17). The evolution of the discharge capacity of p- or n-doped germanium coatings is similar, whatever the current density, but the capacity of the nondoped Ge coating decreases more strongly with increasing the current. For the nondoped germanium, the curve also shows a strange behavior: for each increase of current intensity, the capacity first decreases during a few cycles and then increases. The first step can be attributed to the internal resistance of the coating, and the following increase should be due to another phenomenon, such as low diffusion, morphology modification, porosity increase, etc.

Figure 17 exhibits the cycle life of the doped or nondoped germanium electrodes. The irreversible capacity is always low. All the

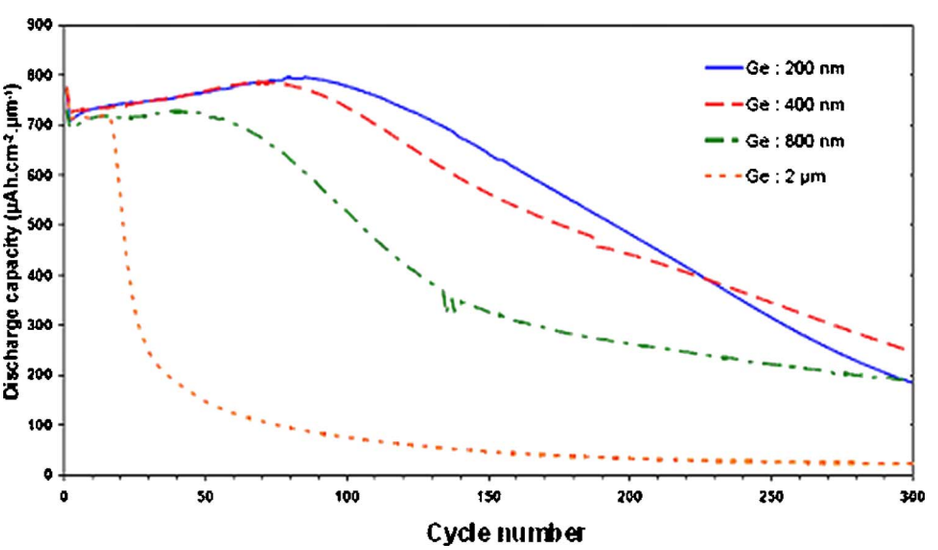

Figure 12. (Color online) Cycling life of p-doped germanium coatings for several thicknesses.

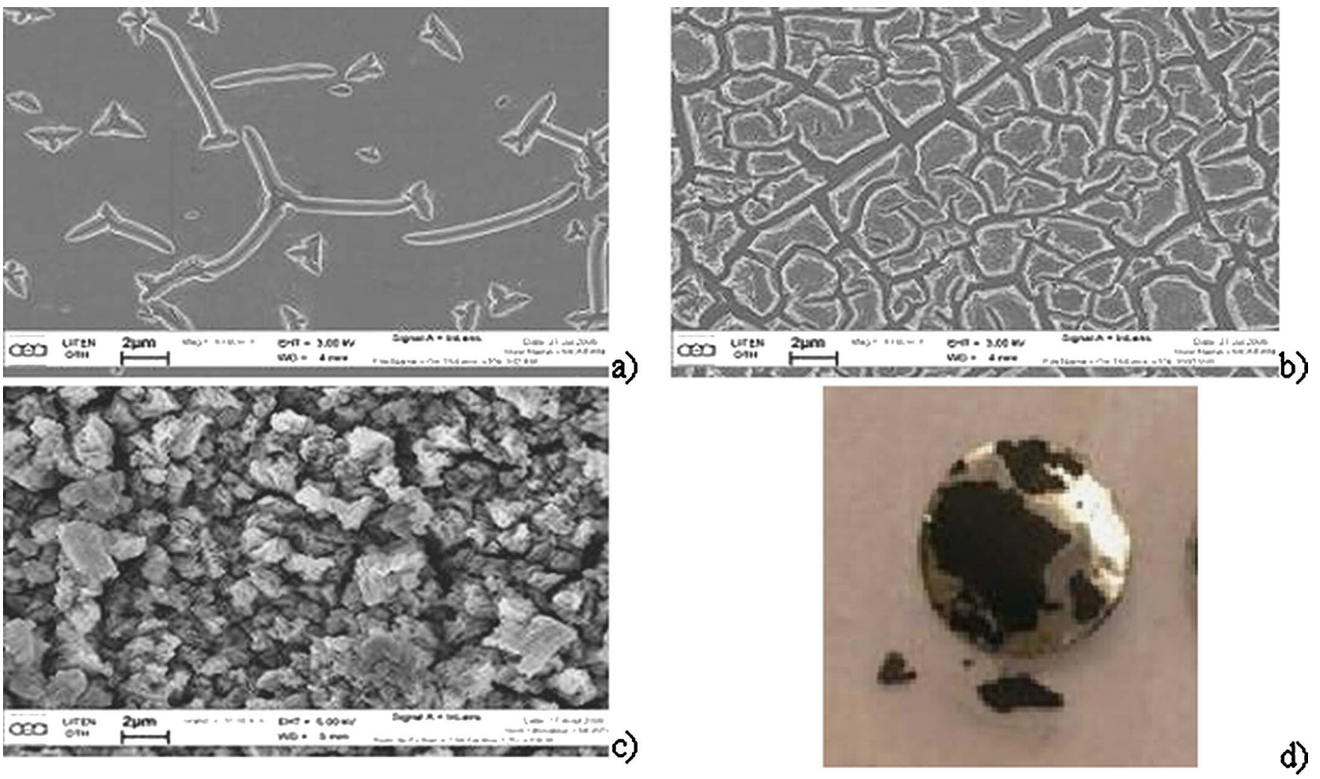

Figure 13. (Color online) SEM micrographs of germanium films after (a) 1, (b) 10, and (c) 110 discharge/charge cycles and optical micrograph of the sample after 300 cycles (d).

curves present the same behavior, i.e., an increase of the capacity during some tens of cycles and then a progressive decrease, more pronounced for the nondoped Ge coating. The best results are obtained for the n-doped coating. Then, n-doping improves the cycling life.

This behavior can be related to the conductivity values of doped or nondoped germanium reported in Table II, in relation with the doping level reported in Table I. As the nondoped germanium coating presents the lower conductivity and the n-doped the higher, these results seem to indicate a correlation between conductivity and cycle life of the coatings.

Discussion

The GITT experiments allow us to measure the diffusion coefficient of Li into Ge. The values are between 5×10^{-12} and 1.75×10^{-10} cm^2 s^{-1}, depending on the doping and the Li rate x into Li_xGe. The diffusion coefficient of Li^+ into silicon varies between $2–3.5 \times 10^{-14}$ and 10^{-13} cm^2 s^{-1}.[17,18] These values are lower than those of germanium, suggesting that germanium could exhibit better lithium insertion properties than Si.

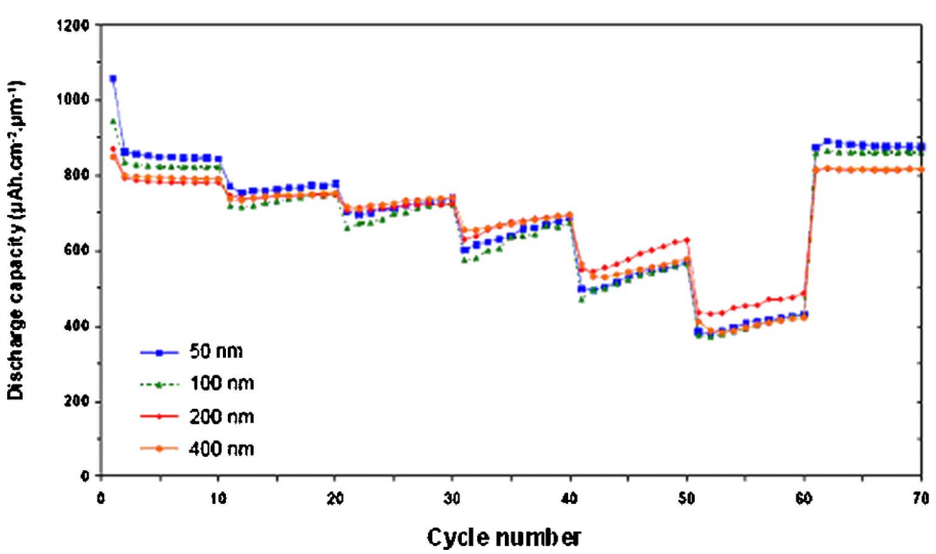

Figure 14. (Color online) Discharge capacities per volume unit of n-doped germanium coatings vs cycle number and for several current densities of several thicknesses.

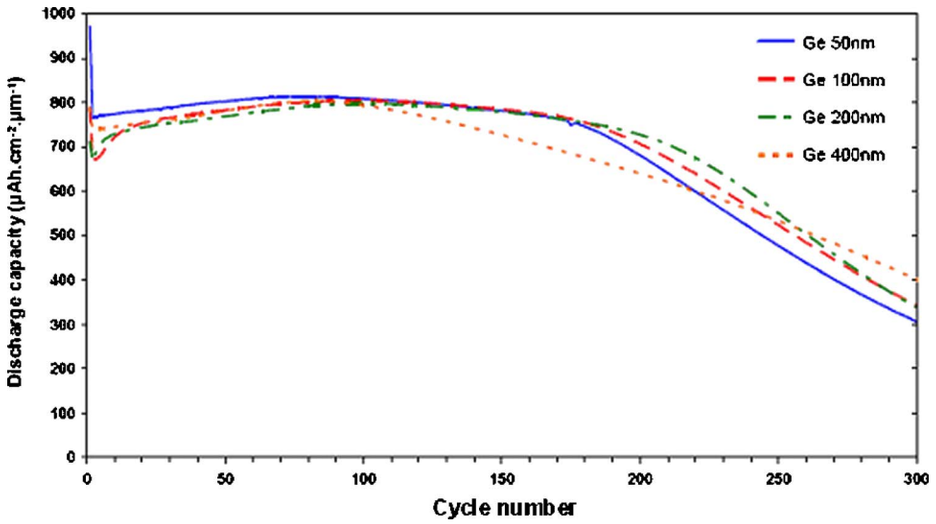

Figure 15. (Color online) Cycling life of n-doped germanium coatings for several thicknesses (50, 100, 200, and 400 nm).

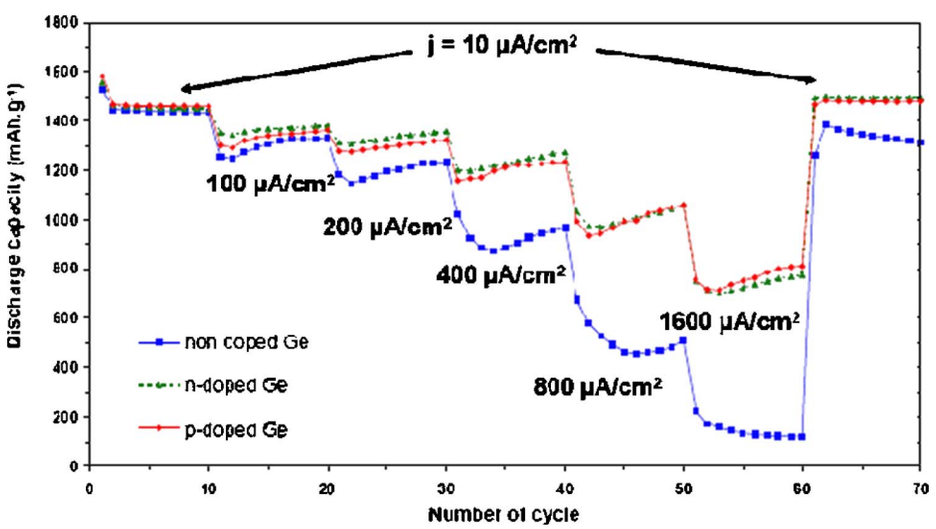

Figure 16. (Color online) Influence of doping germanium on discharge capacities per volume unit vs cycle number and for several current densities.

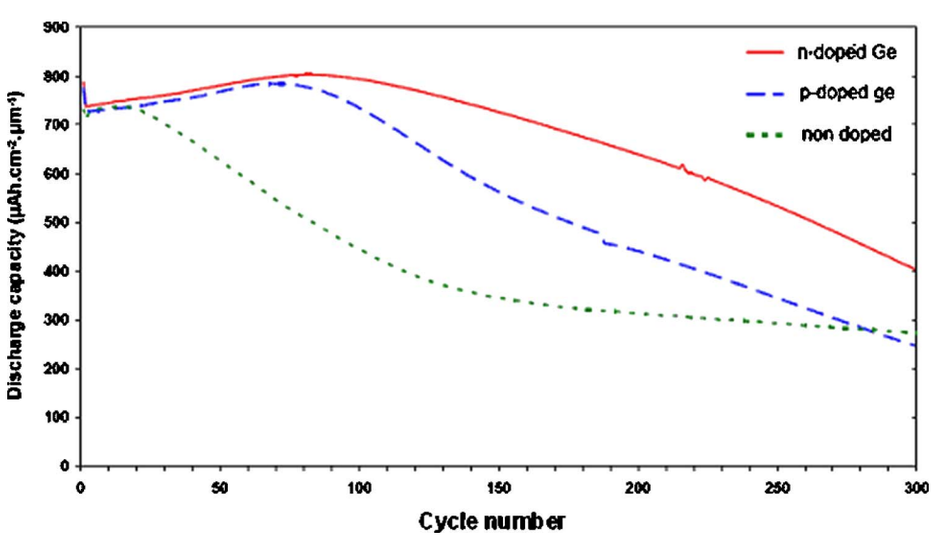

Figure 17. (Color online) Influence of the doping on the cycling life of a 400 nm thick germanium electrode.

Table II. Conductivities of nondoped and doped germanium coatings (1 μm thick).

Doping	Nondoped	p-doped	n-doped
Conductivity (mS cm^{-1})	>1.25	5.7	30

The measured diffusion coefficients of Li^+ into Ge have to be compared to the extrapolated values calculated from the Fuller and Severiens[8] equation

$$D = 25 \times 10^{-4} \exp\left(\frac{-11{,}800}{RT}\right)$$

where R is universal gas constant (cal mol^{-1} K^{-1}) and T temperature (K).

At 300 K, the calculated diffusion coefficient is 6.4×10^{-12} s^{-1}, which is lower than that measured with $x \sim 0$ but very close to that measured for lithiated compound. Differences between calculations and measurements could be explained by the origin of the Fuller and Severiens[8] equation, which was determined by extrapolating their measurements above 423 K. Diffusion coefficient measurements are very fussy experiments, and then, the error factor is relatively high. The differences between doped and nondoped germanium are important at a low rate of Li. The higher the conductivity is, the higher the diffusion coefficient is. This is in agreement with the calculations,[7] which demonstrate that the diffusion coefficient is dependent on the conductivity (Table II).

The voltage profiles prove the existence of some phase transitions during lithiation and delithiation, which are similar to Graetz's results[3,6] (Fig. 6). The presence of several peaks also suggests the formations of different Li–Ge phases during cycling. The plateau corresponding to a two-phase region observed around ~0.5 V during lithiation means that at least one Li–Ge crystalline phase is formed during lithiation. During delithiation, there is only one single-phase region. It probably means that delithiated germanium is amorphous. Electrochemical lithiation seems to enhance the crystallinity of the material, which may be attributed to the high diffusion coefficient of Li^+ into Ge. For thick samples, the crystallization appears only after several cycles, which implies that germanium should get organized gradually. As shown in Fig. 7, a peak appears only during the first discharge and a large irreversible capacity is observed for the initial cycle. It can be due to the formation of a passive layer: the SEI. The SEI is formed at ~0.6 V by the reaction of lithium with the electrolyte during the first lithiation of the germanium electrode (Fig. 11).

A comparison of Fig. 11, 14, and 16, displays different behaviors as a function of the coating thickness. Whatever the thickness of n- and p-doped germanium coatings up to 400 nm, no significant difference can be observed in the evolution of capacity with the current density. A decrease of the coating performance appears for thicknesses of 800 and 400 nm, for p-doped and nondoped germanium coatings respectively. The best is the conductivity or diffusion coefficient, the less sensitive to the thickness are the samples. Then it seems that the limiting factor for thick samples is the diffusion of electrons or lithium. The most famous example of electrode limited by electron diffusion is the case of $LiFePO_4$, whose conductivity is $\sim 10^{-6}$ mS cm^{-1}.[19,20] Although the diffusion coefficient of Li^+ is also lower than into germanium ($\sim 10^{-14}$ cm^2 s^{-1}), the conductivity is very low compared to that of germanium, which ranges between 1 and 30 mS cm^{-1}. It probably means that the limiting factor for Ge electrodes is not electron diffusion but lithium diffusion. High rate capacities (50 C) are ~50% that of low rate capacities for n-doped germanium.

For cycling life, the typical behavior is a low irreversible capacity (at ~10%), an increase or a stability of the capacity during the first cycles, and then a decrease. The best results are obtained with thin n-doped electrodes, which also present the best conductivity, with an increase of the capacity during 180 cycles (Fig. 15).

Conclusion

Germanium coatings have been studied as electrode material for microbatteries in terms of structural and electrochemical properties. As-deposited germanium coatings are amorphous, but crystalline Li–Ge phases are formed during the battery cycling. The diffusion coefficient has been determined by GITT at $\sim 10^{-10}$ cm^2 s^{-1} vs lithium rate into Li_xGe phases. The influence of the doping element nature and concentration, and that of the electrodes thickness have been studied. For the reversible capacities, the best results are obtained for 200 nm thick n-doped germanium coatings. Apart from the capacity loss of the first cycle, the capacity is stable during ~180 cycles at 780 μAh cm^2 μm^{-1} (~1465 mAh g^{-1}). Then the reversible capacity is 91% of the theoretical one. In this work, the good cycling stability, the low irreversibility, and the high diffusion coefficient of Li into germanium have been demonstrated, suggesting that germanium could be a very good electrode material for thin-film microbatteries.

Centre d'Energie Atomique assisted in meeting the publication costs of this article.

References

1. L. Y. Beaulieu, K. C. Hewitt, R. L. Turner, A. Bonakdarpour, A. A. Abdo, L. Christensen, K. W. Eberman, L. J. Krause, and J. R. Dahn, *J. Electrochem. Soc.*, **150**, A149 (2003).
2. N. M. Obrovac and L. J. Krause, *J. Electrochem. Soc.*, **154**, A103 (2007).
3. J. Graetz, C. C. Ahn, R. Yazami, and B. Fultz, *Electrochem. Solid-State Lett.*, **6**, A194 (2001).
4. G. Cho, B. L., W. Sin, K. Cho, K. Kim, and H. Ahn, *J. Alloys Compd.* (2007), doi: 10.1016/j.jallcom.2006.02.099.
5. M. Kim, S. Ahn, J. Park, and J. A. Ascencio, *J. Korean Phys. Soc.*, **49**, 1107 (2006).
6. J. Graetz, C. C. Ahn, R. Yazami, and B. Fultz, *J. Electrochem. Soc.*, **151**, A698 (2004).
7. M. W. Valenta and C. Ramasastry, *Phys. Rev.*, **106**, 73 (1957).
8. C. S. Fuller and J. C. Severiens, *Phys. Rev.*, **96**, 21 (1954).
9. J. F. Pierson, A. Billard, T. Belmonte, H. Michel, and C. Frantz, *Thin Solid Films*, **347**, 78 (1999).
10. P. Briois, F. Lapostolle, V. Demange, E. Djurado, and A. Billard, *Surf. Coat. Technol.*, **160**, 821 (2007).
11. F. Kong, R. Kostecki, G. Nadeau, X. Song, K. Zaghib, K. Kinoshita, and F. McLarmon, *J. Power Sources*, **97**, 58 (2001).
12. R. Nesper, *Prog. Solid State Chem.*, **20**, 1 (1990).
13. Q. C. Johnson, G. S. Smith, and D. Wood, *Acta Crystallogr.*, **18**, 131 (1965).
14. B. Predel, *Landolt-Börnstein Group IV Physical Chemistry*, Vol. 5 F, p. 154, Springer, Berlin (1996).
15. V. Hopf, W. Müller, and H. Schäfer, *E. Naturforsch.*, **27b**, 1157 (1972).
16. J. S. Bae and S. I. Puyn, *Solid State Ionics*, **90**, 251 (1996).
17. T. L. Kulova, Y. V. Pleskov, A. M. Skundin, E. I. Terukov, and O. I. Kon'kov, *Russ. J. Electrochem.*, **42**, 791 (2007).
18. E. M. Pell, *Phys. Rev.*, **119**, 1222 (1960).
19. P. S. Herle, B. Ellis, N. Coombs, and L. F. Nazar, *Nat. Mater.*, **3**, 147 (2004).
20. C. Delacourt, C. Wurm, L. Laffont, J.-B. Leriche, and C. Masquelier, *Solid State Ionics*, **177**, 333 (2006).